

# Region Specific Consideration for GMPE Development, Representative Seismic Hazard Estimation and Rock Design Spectrum for Himalayan Region



P. Anbazhagan  and Ketan Bajaj

## 1 Introduction

The current seismic hazard analysis (SHA) of any earthquake-prone area is practically bending towards the development and selection of a regional ground motion prediction equation (GMPE). Additionally, improvement in the seismic networks and geophysical testing resulted in the advancement of the functional form of GMPE by incorporating various site and source parameters. GMPE models describe the distribution of ground motion in terms of median and logarithmic standard deviation (Strasser et al., 2009). The general procedure used in developing any GMPE is the regression analysis of the ground motion recordings either from past events or stochastic simulation. To date, various guidelines and tools are available for selecting a suitable GMPE for any seismic study area. Despite the availability of various methods and criteria for choosing an appropriate GMPE (Cotton et al., 2006; Scherbaum et al., 2009) for many practical applications, there exists an important issue regarding the applicability of a GMPE developed for one region to another region. A vital step in any SHA is the selection of suitable GMPEs based on the region-specific parameters. GMPEs are widely used for predicting the level of ground shaking in terms of Peak Ground Acceleration (PGA), Spectral Acceleration (SA) etc., corresponding to magnitude (moment magnitude, in most of the cases), distance (epicentral or hypocentral), site condition and type of faulting of any site. The essential element of any Probabilistic Seismic Hazard Analysis (PSHA) is an integration of a suitable ground motion model for the determination of ground motion parameters of a given site for each earthquake scenario.

---

P. Anbazhagan (✉)

Department of Civil Engineering, Indian Institute of Science, Bengaluru, Karnataka, India  
e-mail: [anbazhagan@iisc.ac.in](mailto:anbazhagan@iisc.ac.in)

K. Bajaj

Swiss Re, Bangalore, Karnataka, India  
e-mail: [ketan\\_bajaj@swissre.com](mailto:ketan_bajaj@swissre.com)

To date, various GMPEs exist worldwide for the determination of seismic hazards at bedrock or ground surface for various tectonic regions, and these GMPEs are compiled by Douglas (2020). Various authors (Anbazhagan & Kumar, 2013; Bajaj and Anbazhagan 2019b; Das et al., 2006; Gupta, 2010; Iyengar & Ghosh, 2004; Nath et al., 2005, 2009; NDMA, 2017; Ramkrishnan et al., 2020; Sharma & Bungum, 2006; Sharma et al., 2009; Singh et al., 1996) have proposed different GMPEs for the Indian subcontinent. NGA-West 2 project has developed a series of ground motions for the tectonically active region of the shallow crustal earthquakes. These GMPEs are proposed by Abrahamson et al. (2014), Boore et al. (2014), Campbell and Bozorgnia (2014), Chiou and Youngs (2014), and Idriss (2014). Recently, Akkar et al. (2014) and Bindi et al. (2014) have developed new GMPEs for the Pan-European region. Moreover, Zhao et al. (2016a, b, c, d) have developed four new GMPEs for Japan by differentiating the subduction interface earthquakes, subduction slab earthquakes, and shallow crustal and upper mantle earthquakes. Zhao et al. (Zhao et al., 2016) method is being used in different hazard analysis studies around the world, especially for subduction tectonic regimes. The GMPEs developed for the NGA-west, and Japan region is widely used to determine seismic hazard for the various regions of the Indian Subcontinent. The attenuation characteristic of the seismic waves for the Himalayan region is different as compared to the western US and Japan (Bajaj, 2018). Hence, identifying proper GMPEs and arriving shape of the design spectrum for the shallow crustal region of the seismically active Himalayan subduction region is mandatory.

In this study, we collected available recorded earthquake data from the Himalayan region. Then these data are processed and used to identify the best possible GMPEs functional form. Further, applicable GMPEs are reviewed and identified as suitable GMPEs for the Himalayan region with the estimation of ranks and weights by adopting a segmented distance of <100 km, 100–300 km, and >300 km as per Anbazhagan et al. (2015). Available recorded data are further used to arrive a cutoff period for acceleration, velocity, and displacement sensitive regions, thereby developing smoothed and normalized design spectrum shape for the Himalayan region.

## 2 Seismic Data and Study Area

Instrumented seismic ground motion records are valuable data to understand many seismological, seismotectonic, and engineering aspects of the earthquake in the region. Even though the Himalayan region has a very long history of seismic activity and catastrophic earthquakes, systematic seismic instrumentation in the Himalayan region and data available for researchers are started very recently. The strong motion data is collected from the strong motion instrumentation network of the Indian Institute of Technology, Roorkee (IITR) and also from Virtual Data Center (VDC). A detailed description of these strong motion accelerographs and data processing of the waveforms are given in Kumar et al. (2012) and Bajaj and Anbazhagan (2019b). Out

of the total 520 seismic ground motion recordings, 252 were collected from the IITR, 68 seismic ground motions recorded before 2005 were collected from VDC, and the rest 200 from the Indian seismic and GNSS network. Out of 520 recordings, 241 are rock recordings, and the remaining 279 are soil recordings. Only rock recordings are used in the present study. The processing of strong-motion data involves baseline-correction, instrumental scaling, and frequency filtering. The strong motion database is processed according to the procedure suggested by Boore and Bommer (2005). The earthquake occurred between 1988 and 2015 with a moment magnitude ( $M_w$ ) of 4.5–7.8, and a hypocentral distance of 10–500 km was compiled. Figure 1 shows the location of the seismic station and the earthquake data collected. These stations cover the Indian Himalayan range from Jammu and Kashmir to Meghalaya. Most of the available recorded earthquakes in the Himalayan region were collected, which cover the Western Part, Central Part, and Eastern Part of North India. This region is responsible for an earthquake disaster in India’s northern part and the north side of the Indo-Australian plate boundary and subduction zone.

Each earthquake record consists of 3 component records of velocity/acceleration time histories. Anbazhagan et al. (2016b) compiled earthquakes above  $M_w$  of 5.0 with an isoseismal map and generated a relationship between Intensity and ground motion and spectral parameters for the Himalayan region. These relations are useful to estimate ground motion and spectral parameters from intensity values, which help to account for old intensity values in seismicity and predict future seismic hazard values. These seismic stations were classified based on the geology of the region,

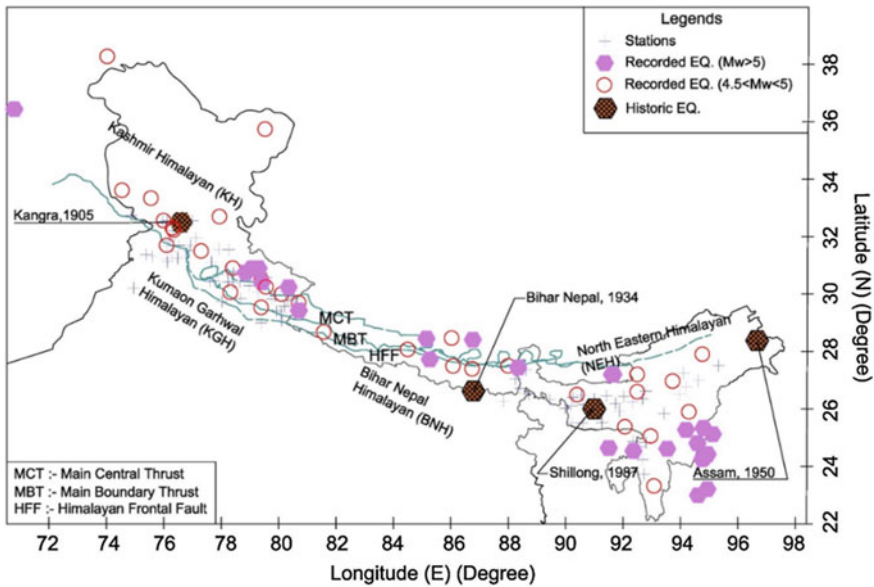


**Fig. 1** The recorded database was used in developing the new ground-motion prediction for the Himalayan region (after Bajaj and Anbazhagan 2019b)

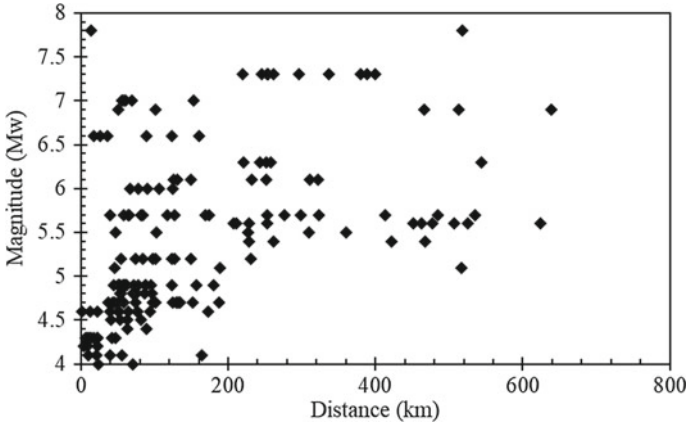


**Fig. 2** Rock site recorded ground motions data used in the study

and no site-specific data were used to characterize them as rock and soil stations. So, Anbazhagan et al. (2019) analysed data systematically, processed by applying baseline-correction and band-pass-filter between 0.75 and 0.9 Hz and 25–27 Hz. These data are used to extract time-domain parameters of peak acceleration/velocity and frequency domain parameters of the corner and cutoff frequencies and predominant frequency through H/V ratio. More about data and seismic station classification can be found in Anbazhagan et al. (2019). Figure 2 shows a plot of rock site data used in the study. These data are further used to identify GMPE functional form, select GMPEs for seismic hazard analysis, and drive the design spectrum for the HR.

### 3 Functional Form and New GMPE

GMPE of the region should reflect the wide range of magnitude, distance, directivity, fault type, etc., to serve various engineering requirements. GMPE model must account for magnitude dependence and saturation, as well as attenuation of stress waves with distance due to spreading and material damping. So GMPE functional form used to regress the recorded data should fulfil the above essential requirement. Many explanatory parameters are necessary for GMPE functional form; that is why NGA-West 2 GMPEs are more complex. Various researchers have used different functional forms for capturing magnitude and distance scaling in GMPEs. To examine the applicability of available functional forms for the Himalayan region where a less recorded strong motion database is available, we reviewed available GMPEs. To date, various GMPEs developed worldwide for the determination of seismic hazards at bedrock or surface for various tectonic regions, and these GMPEs are compiled by Douglas (2020). Douglas started compiling GMPEs from 2000 onwards and group them based on several criteria with highlighted applicability and limitations. He is

updating every year and publishing reports on GMPEs (<http://www.gmpe.org.uk/>), a recent report is Douglas (2020). Applicable GMPEs for the Himalayan region (HR) were summarized by Bajaj and Anbazhagan (2021a) and they are updated here. Table 1 shows these applicable GMES for HR with the short form.

HR GMPEs can be divided into two major groups i.e., developed for HR, India, and developed elsewhere (NGA-West 2, Pan-European, and Japan GMPEs), applicable to HR. GMPEs applicable for HR can be grouped as magnitude scaling and distance scaling based on functions used in the GMPEs. Recorded rock site data is used to get GMPE coefficients for different functional forms applicable to the HR region. Further, the compatibility of various functional forms for distance and magnitude scaling using the mixed-effect regression of residual calculated from different functional forms. Based on that, uncertainties have been evaluated concerning distance and magnitude ranges within the event and between events. The whole algorithm and different functional form used is explained in detail and presented in Bajaj and Anbazhagan (2018, 2019a). Based on region-specific analysis and data, the representing functional form of HR is given below:

$$\ln Y = a_1 + a_2(M - 6) + a_3(9 - M)^2 + a_4 \ln R + a_m \ln R(M - 6) + a_7 R + \sigma \quad (1)$$

where,  $\ln Y$ ,  $M$ ,  $R$ , and  $\sigma$  are respectively logarithm of ground motion, magnitude, hypocentral distance, and standard deviation and  $a_1$ ,  $a_2$ ,  $a_3$ ,  $a_4$ ,  $a_m$  and  $a_7$  are the corresponding regression coefficients. The coefficient  $a_m$  is equal to  $a_5$  when  $M_w < 6.0$  and  $R < 300$ , else is equal to  $a_6$ . It can be noted here that many of GMPE developed for HR considering functional form other than Eq. (1) has a considerable bias. PGA is more biased in the case of AN13, NA09, and SH09 as compared to NDMA10 and GU10. In some cases, like ID14, CY14, NDMA10, and AN13, bias is less for long periods. Many recent GMPEs not developed for HR have less bias than GMPEs developed for HR. Hereby we suggest any GMPEs for HR can be developed by considering the functional form given in Eq. (1).

### 3.1 Regional Seismotectonic Parameters and GMPE

The Himalayan region has a smaller number of GMPEs when compared to similar active seismic areas in the world. Moreover, most GMPEs are developed with lots of assumptions or seismotectonic parameters of another region in the world. This may be due to a smaller number of recorded earthquake data in the region. Anbazhagan et al. (2013) summarized GMPEs developed up to 2013 for HR and widely used GMPEs in HR studies but not developed for the region. The authors concluded that most of the GMPEs developed for the HR area are only applicable for limited range magnitude and distance. GMPEs developed for HR are incapable of predicting hazard values close to highly ranked GMPEs for the entire distance range of interest. Also, many of HR GMPEs were developed using seismological model parameters

**Table 1** Available GMPEs considered for seismic hazard analysis of the IGB

S. no	GMPE	Abbreviation	Magnitude range	Distance range
<i>Himalayan GMPE</i>				
1	Singh et al. (1996)	SI_96	5.7–7.2	≤100
2	Iyengar and Gosh (2004)	IYGO_05	5.0–8.0	≤100
3	Nath et al. (2005)	NA_05	3–8.5	≤100
4	Sharma and Bungum (1459)	<b>SHBU_06</b>	5.5–7.2	≤300
5	Das et al. (2006)	DA_06	4.6–7.6	≤200
6	Nath et al. (2009)	<b>NA_09</b>	4.8–8.1	≤ 100
7	Sharma et al. (2009)	<b>SH_09</b>	5.2–6.9	≤100
8	NDMA (2017)	<b>NDMA_10</b>	6.3–7.2	150–375
9	Gupta (2010)	GU_10	4–8.5	≤500
10	Anbazhagan et al. (2013)	<b>AN_13</b>	5.3–8.7	≤300
11	Bajaj and Anbazhagan (2019b)	<b>BAN_19</b>	4.0–9.0	≤750
12	Ramabhadran et al. (2020)	RAM_20	4.2–6.9	<640
<i>Similar region GMPE</i>				
13	Abrahamson and Litehiser (1989)	ABLI_V_89	5–8	≤100
14	Abrahamson and Litehiser (1989)	ABLI_H_89		
15	Youngs et al. (1997)	YO_97	≥ 5	10–500
16	Campbell (1997)	CAM_H_97	4–7.8	3–60
17	Campbell (1997)	CAM_V_97		
18	Spudich et al. (1999)	SP_99	5–7.7	≤200
19	Atkinson and Boore (2003)	ATB_03	≥ 6.5	40–200
20	Takahashi et. al. (1271)	TA_04	5–8.3	≤300
21	Ambraseys et al. (2005)	AMB_05	> 5.0	≤100
22	Kanno et al. (2006)	<b>KA_06</b>	≥ 5.5	≤200
23	Zhao et al. (Zhao, Zhang, et al., 2016)	<b>ZH_06</b>	5–8.0	≤200
24	Campbell and Bozorgnia (2008)	CABO_08	4.0–8.5	≤200
25	Idriss (2008)	ID_08	4–8.0	≤200
26	Boore and Atkinson (2008)	BOAT_08	5–8	≤200
27	Chiou and Youngs (2008)	CY_08	4.0–8.5	≤200 km
28	Abrahamson and Silva (2008)	ABSI_08	5–8.5	≤200
29	Lin and Lee (2008)	LL_08	5.2–7.9	≥60
30	Cauzzi and Faccioli (2008)	<b>CAFA_08</b>	5.0–6.9	
31	Aghabarati and Tehranizadeh (2009)	AGTH_08_09_H	5.3–8.1	15–630

(continued)

**Table 1** (continued)

S. no	GMPE	Abbreviation	Magnitude range	Distance range
32	Aghabarati and Tehranizadeh (2009)	AGTH_08_09_V		
33	Akkar and Bommer (2010)	AKBO_10	5–7.6	≤100
34	Akkar et al. (2014)	<b>AK_14</b>	4.0–8.0	≤200
35	Bindi et al. (2014)	<b>BI_14</b>	4.0–7.6	≤300
36	Abrahamson and Silva (2014)	<b>ABSI_14</b>	3.0–8.5	≤300 km
37	Boore et al. (2014)	<b>BA_14</b>	3.0–8.5	≤400 km
38	Campbell and Bozorgnia (2014)	<b>CABO_14</b>	3.0–8.5	≤500
39	Chiou and Youngs (2014)	<b>CY_14</b>	3.0–8.0	≤100 km
40	Akkar and Sandikkaya (2014)	<b>ID_14</b>	≥ 5.0	≤100 km
41	Zhao et al. (2016a)	ZH_16_SI	4.5–8.0	≤300 km
42	Zhao et al. (2016b)	ZH_16_SS	4.5–8.0	≤300 km
43	Zhao et al. (2016c)	<b>ZH_16_CM</b>	4.5–8.0	≤300 km

developed in other countries. Bajaj and Anbazhagan (2019b) tried for the first time to estimate seismological model parameters using HR region earthquake data discussed earlier. Authors derived geometric spreading and an elastic attenuation using Fourier Amplitude Spectrum (FAS) by dividing HR as Kashmir Himalayan (KH), Kumaon-Garhwal Himalayan (KGH), Bihar-Nepal Himalaya (BNH), and Northeastern part of the Himalayan region (NEH). The stress drop and duration model for HR was established first time using available data. A stress drop was observed with a kink point at 5.5 Mw through the bilinear model. Regional recorded data shows that the duration model broke at 60 km hypocentral distance and helped arrive first time duration model beyond 700 km. Here, the authors also proved that Japan and California's widely used duration model is nowhere close to the regional model. Most of the existing duration models are applicable only up to 300 km. Bajaj and Anbazhagan (2019b) systematically arrived at seismotectonic parameters for most of the historic major earthquakes in HR from literature and calculation.

Even though we have a good amount of data (Fig. 2) to arrive at the seismotectonic parameters of the region still, these are insufficient to cover the entire spectrum of magnitudes and distances required for GMPE development. It can also be noted that many seismologists highlighted the seismic gaps in the study area. Bilham (2015) studied the potential slip in the range of 9–14 m with the expected earthquake as large as 8.9 Mw in the Kashmir Himalayan region. Moderate earthquakes with Mw > 6 that have occurred from 1900 to 2000 in the Kumaon- Garhwal Himalayan region reflect the high seismicity in the area and the possibility of recurrence of large earthquakes in the future (Srivastava et al., 2015). Srivastava et al. (2015) demarked the whole Himalayan region into 10 seismic gaps by studying the micro-seismicity, paleo-seismicity, Global Positioning System, and variation in local tectonics. They

concluded that the Himalayan region is not equally seismogenic to produce a magnitude of 8.5 Mw and above. Here it is very clear that HR has many potential sources that can cause greater earthquakes above Mw of 8 and may results in several seismic geohazards in the Himalayan and Indo-Gangetic Basin (IGB) beyond 300 km. Table 1 and Fig. 2 clearly show that region-specific robust GMPEs are available up to 2019 for the region to arrive at possible future seismic hazards. Bajaj and Anbazhagan (2019b) systematically compiled seismotectonic parameters of different past earthquakes and used them to simulate ground motion by adopting Motazedian and Atkinson (2005) procedure by considering new seismological model parameters arrived from regional data. The authors initially simulated time history at recorded seismic stations and validated, then repeated the same 0.1-unit step distance for a distance of 10–750 km by adopting the apparent station concept. The mixed-effect regression analysis was carried out by authors considering the combined set of recorded and region-specific simulated data using the GMPE functional form given in Sect. 2. Figure 3 shows the comparison of new GMPEs with existing GMPEs widely used in hazard analysis of HR for the major Magnitude of 8.7 (maximum reported 1950 Assam–Tibet earthquake) for rock level. This can be observed that the current GMPE is predicting SA values in between crustal GMPEs developed by NGA. NDMA10 (2017) is a widely used GMPE in most of the hazard studies in India and predicts low values for large earthquakes compared to HR GMPEs.

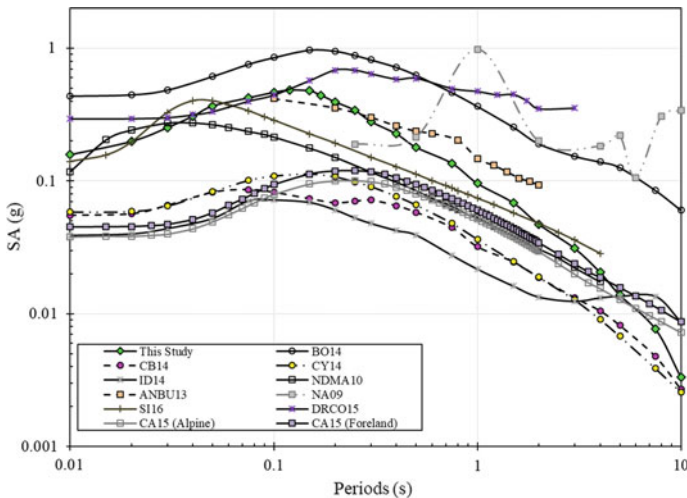


**Fig. 3** Comparison of new GMPEs with other active crustal GMPEs for magnitude of 8.7 and hypocentral distance of 150 km

## 4 Ranks and Weights of GMPEs for HR

Predictive models/equations for peak ground and spectral acceleration are a requirement for seismic hazard analysis. Most representatives of such equations for HR are less when compared to the similar seismically active regions in the world. In this study, in order of rank and weight GMPEs applicable to HR using recorded data, we have updated compiled GMPEs by Anbazhagan et al. (2013) and also recently developed in the region by Bajaj and Anbazhagan (2019b). Even though, as of now, 15 GMPEs were developed for the study area, only 4 GMPEs marked can be used for both deterministic and probabilistic Seismic Hazard Analysis (SHA) within the specified applicable range. Among these 43 GMPEs, only marked in italic bold in Table 1 can be used to arrive uniform hazard spectrum as other GMPEs don't have coefficients for spectral acceleration at a different period. Table 2 shows GMPEs applicable to the study with spectral acceleration coefficient for the zero period. In order to model uncertainty through a logic tree approach, we need a larger number of GMPEs, so it is necessary to include applicable GMPEs developed for similar seismotectonic regions.

Narrowing down the most appropriate GMPEs to the region is essential for reliable SHA and representative PGA and SA estimation. Various authors have given quantitative (Delavaud et al., 2009; Scherbaum et al., 2009) and qualitative (Bommer et al., 2010; Cotton et al., 2006) approaches for selecting the GMPE. In this study, both approaches are used. In total, 43 GMPEs are considered suitable for the HR for the analysis using the criteria proposed by Bommer et al. (2010). Scherbaum et al. (2009) and Delavaudet al. (2009) defined an information-theoretic approach that makes use of average sample log-likelihood (LLH) for ranking the available GMPE of a study area. LLH is defined as

$$LLH(g, x) = -\frac{1}{n} \sum_{i=1}^n \log_2(g(x_i)) \quad (3)$$

where,  $x = \{x_i\}$ ,  $i = 1, \dots, N$  are the empirical data and  $g(x_i)$  is the likelihood that model  $g$  has produced the observation  $x_i$ . Here  $g$  is the probability density function given by GMPE to predict the observation produced by an earthquake with a magnitude  $M_w$  and distance  $R$  for the source (Delavaud et al., 2012). LLH values are used to rank the GMPEs and the low LLH value indicates a better ranking. Further, to determine the weight of each GMPE, Delavaudet al. (2012) defined the weight factor and data support index (DSI). The weight and DSI are defined as

$$w_i = \frac{2^{-LLH(g_i, x)}}{\sum_{k=1}^n 2^{-LLH(g_k, x)}} \quad (4)$$

$$DSI_i = 100 \frac{w_i - w_{unif}}{w_{unif}} \quad (5)$$

**Table 2** List of GMPEs used in the study for LLH calculations

Sl no.	Abbreviation of the equation	Standard form of equation	Coefficients value for zero periods
1	SHBU-06	$\ln(A) = c_2 M - \ln \left[ X + \exp(c_3 M) \right],$ <p>Where, <math>A</math> is spectral acceleration in g</p>	$c_2 = 0.8295,$ $b = 1.2,$ $c_3 = 0.5666$
2	NATH-09	$\ln(PSA) = c_1 + c_2 M + c_3 (10 - M)^3 + c_4 \ln(r_{rup} + c_5 \exp^6 M),$ <p>Where, <math>PSA</math> is peak spectral acceleration in g</p>	$c_1 = 9.143, c_2 = 0.247,$ $c_3 = -0.014,$ $c_4 = -2.697,$ $c_5 = 32.9458, c_6 = 0.0663$
3	SH-09	$\log(A) = b_1 + b_2 M + b_3 \log \left( \sqrt{R_{fB}^2 + b_4^2} + b_5 S + b_6 H \right),$ <p>Where, <math>A</math> is spectral acceleration in <math>m/s^2</math></p>	$b_1 = 1.0170, b_2 = 0.1046,$ $b_3 = -1.0070, b_4 = 15 \text{ km},$ $b_5 = -0.0735, b_6 = -0.3068$ $S = 1$ for rock site and 0 for other case, $H = 1$ for strike slip mechanism and 0 for other cases
4	NDMA-10	$\ln(PSA) = c_1 + c_2 M + c_3 M^2 + c_4 R + c_5 \ln \left[ R + c_6 \exp(c_7 M) \right] + c_8 \ln(R) f_o$ <p>Where, <math>PSA</math> is peak spectral acceleration in g,  <math>f_o = \max \left( \ln \left( \frac{R}{100} \right), 0 \right)</math></p>	$c_1 = -3.7438, c_2 = 1.0892,$ $c_3 = 0.0098,$ $c_4 = -0.0046,$ $c_5 = -1.4817, c_6 = 0.0124,$ $c_7 = 0.9950, c_8 = 0.1249$

(continued)

**Table 2 (continued)**

Sl no.	Abbreviation of the equation	Standard form of equation	Coefficients value for zero periods
5	ANBU-13	$\log(y) = c_1 + c_2 M - b \log(X + e^{c_3 M}) + \sigma$ <p>Where y is SA in g, X is the hypocentral distance in km</p>	$c_1 = -1.283,$ $c_2 = 0.544,$ $c_3 = 0.381, b = 1.792$
6	ZH_06	$\ln(y) = aM + bX - \ln(r) + e(h - h_c)\delta_h + F_R$ $r = X + c \exp(dM)$ <p>Where, y is peak spectral acceleration in cm/s<sup>2</sup></p>	$a = 1.101$ $b = -0.00564$ $c = 0.0055$ $d = 1.080$ $e = 0.01412$
7	KA_06	<p>If <math>d &lt; = 30</math> km</p> $\log(\text{Pre}) = a_1 M + b_1 X - \log\left(X + d_1 \cdot 10^{\left(e^{1 M_w}\right)}\right) + c_1$ <p>If <math>d &gt; 30</math> km</p> $\log(\text{Pre}) = a_2 M + b_2 X - \log(X) + c_2$ <p>Where Pre is peak spectral acceleration in cm/s<sup>2</sup></p>	$a_1 = 0.56$ $b_1 = -0.0031$ $c_1 = 0.26$ $d_1 = 0.0055$ $e_1 = 0.37$ $c_2 = 1.56$ $a_1 = 0.41$ $b_1 = -0.0039$
8	CAFA_08	$\log_{10} y = a_1 + a_2 M_w + a_3 \log_{10} R + a_B S_B + a_C S_C + a_D S_D$ <p>Where, y is in m/s<sup>2</sup></p> <p>A – Rock like <math>V_{s30} &gt; 800</math> m/s, <math>S_B = S_C = S_D = 0</math></p> <p>B – Stiff ground <math>360 \leq V_{s30} &lt; 800</math> m/s, <math>S_B = 1, S_C = S_D = 0</math></p> <p>C – <math>180 \leq V_{s30} &lt; 360</math> m/s <math>S_B = 0, S_C = 1, S_D = 0</math></p> <p>D – Very soft ground <math>V_{s30} &lt; 180</math> m/s, <math>S_B = 0, S_C = 0, S_D = 1</math></p>	$a_1 = -1.296$ $a_2 = 0.556$ $a_3 = -1.582$ $a_B = 0.22$ $a_C = 0.304$ $a_D = 0.332$

(continued)

**Table 2 (continued)**

Sl no.	Abbreviation of the equation	Standard form of equation	Coefficients value for zero periods
9	AK_14	$\ln Y = \ln Y_{REF} + \ln S + \varepsilon \sigma$ $\ln Y_{REF} = \begin{cases} a_1 + a_2(M - 6.75) + a_3(8.5 - M)^2 + [a_4 + a_5(M - 6.75)] \\ \quad \ln \sqrt{R^2 + a_6^2} + a_8 F_N + a_9 F_R + SM_W \leq 6.75 \\ a_1 + a_7(M - 6.75) + a_3(8.5 - M)^2 + [a_4 + a_5(M - 6.75)] \\ \quad \ln \sqrt{R^2 + a_6^2} + a_8 F_N + a_9 F_R + SM_W > 6.75 \end{cases}$ $\ln S = \begin{cases} b_1 \ln(V_{s,30}/V_{REF}) + b_2 \ln \left[ \frac{PGA_{REF} + c(V_{s,30}/V_{REF})^n}{(PGA_{REF} + c)(V_{s,30}/V_{REF})^n} \right] \text{ for } V_{s,30} \leq V_{REF} \\ b_1 \ln \left[ \frac{min(V_{s,30}, VC_{ON})}{V_{REF}} \right] \text{ for } V_{s,30} > V_{REF} \end{cases}$ <p>Where, Y is in g  lnS = is the non-linear site amplification factor  R may be <math>R_{JB}</math>, <math>R_{epi}</math> or <math>R_{hsp}</math> and according the coefficient varies  For strike-slip fault, <math>F_N = F_R = 0</math>  For Normal fault, <math>F_N = 1, F_R = 0</math>  For reverse fault, <math>F_N = 0, F_R = 1</math>  <math>\Phi</math>, <math>\tau</math> and <math>\sigma</math> are intra-event, inter-event and total standard deviation respectively</p> $PGA_{REF} = \begin{cases} 0.273722398 \text{ for } R_{JB} \\ 0.418813071 \text{ for } R_{epi} \\ 0.579508611 \text{ for } R_{hsp} \end{cases}$	$a_1 = 3.26685$ $a_2 = 0.0029$ $a_3 = -0.04846$ $a_4 = -1.47905$ $a_5 = 0.2529$ $a_6 = 7.5$ $a_7 = -0.5096$ $a_8 = -0.1091$ $a_9 = 0.0937$ $b_1 = -0.41997$ $b_2 = -0.288846$ $\Phi = 0.6475$ $\tau = 0.3472$ $\sigma = 0.7347$ $V_{REF} = 1000$ $VC_{ON} = 750$ $c = 2.5$ $n = 3.2$

(continued)

**Table 2 (continued)**

Sl no.	Abbreviation of the equation	Standard form of equation	Coefficients value for zero periods
10	BL_14	$\ln Y = e_1 + F_D + F_M + F_S + F_{Sof}$ $F_D = [c_1 + c_2(M - 5.5)] \log(\sqrt{R^2 + h^2} / R_{REF}) - c_3(\sqrt{R^2 + h^2} - R_{REF})$ $F_M = \begin{cases} b_1(M - 6.75) + b_2(M - 6.75)^2 & \text{for } M_w \leq 6.75 \\ b_3(M - 6.75) & \text{for } M_w > 6.75 \end{cases}$ $F_{Sof} = f_j E_j$ <p>Where, <math>j = 1, 2, 3</math> and 4 for normal, reverse, strike-slip and unspecified faults  <math>F_S = \gamma \log(V_{S30}/800)</math> if <math>V_{S30}</math> is used  <math>F_S = s_j C_j</math> if used site class is used                      Where, <math>C_j</math> is the dummy variable  <math>j = 1, 2, \&amp; 4</math> for site class A,B,C&amp;D  <math>C_j = 0</math>  <math>R = R_{JB}</math>, i.e., Joyner-Boore distance  <math>R_{REF} = 1</math> km</p>	$e_1 = 3.45078$ $c_1 = -1.36061$ $c_2 = 0.215873$ $c_3 = 0.000733$ $h = 6.14717$ $b_1 = -0.02087$ $b_2 = -0.07224$ $b_3 = 0$ $f_1 = -0.03228$ $f_2 = 0.073678$ $f_3 = -0.01943$ $f_4 = 0$ $\tau = 0.180904$ $\theta = 0.276335$ $\sigma = 0.330284$ $s_1 = 0$ $s_2 = 0.137715$ $s_3 = 0.233048$ $s_4 = 0.214227$

(continued)

**Table 2 (continued)**

Sl no.	Abbreviation of the equation	Standard form of equation	Coefficients value for zero periods
11	ABSI_14	$\ln Sa = f_1 + F_{RV}f_7 + F_N f_{11} + f_5 + F_{HW}f_4 + f_6 + f_{10} + \text{Regional}$ $f_1 = \begin{cases} a_1 + a_5(M - M_1) + a_8(8.5 - M)^2 + [a_2 + a_3(M - M_1)]\ln R + a_{17}rup & M \geq M_1 \\ a_1 + a_4(M - M_1) + a_8(8.5 - M)^2 + [a_2 + a_3(M - M_1)]\ln R + a_{17}rup & M_2 \leq M < M_1 \\ a_1 + a_4(M_2 - M_1) + a_8(8.5 - M)^2 + a_6(M - M_2) + a_7(M - M_2)^2 + [a_2 + a_3(M - M_1)]\ln R + a_{17}rup & M < M_2 \end{cases}$ $R = \sqrt{rup^2 + c_{4M}^2}$ $c_{4M} = \begin{cases} c_{4M} > 5 \\ c_4 - (c_4 - 1)(5 - M)/4 < M \leq 5 \\ 1, M < 4 \end{cases}$ $f_7 = \begin{cases} a_{11}M > 5 \\ a_{11}(M - 4)/4 < M \leq 5 \\ 0, M < 4 \end{cases}$ $f_8 = \begin{cases} a_{12}M > 5 \\ a_{12}(M - 4)/4 < M \leq 5 \\ 0, M < 4 \end{cases}$	$c_4 = 4.5$ $M_1 = 6.75$ $M_2 = 5$ $a_1 = 0.587$ $a_2 = -0.790$ $a_3 = 0.275$ $a_4 = -0.1$ $a_5 = -0.41$ $a_6 = 2.154$ $a_8 = -0.015$ $a_{10} = 1.735$ $a_{11} = 0$ $12 = -0.1$ $a_{13} = 0.6$ $a_{14} = -0.3$ $a_{15} = 1.1$ $a_{17} = -0.0072$ $a_{43} = 0.1$ $a_{44} = 0.05$ $a_{45} = 0$ $a_{46} = -0.05$ $a_{25} = -0.015$ $a_{28} = 0.0025$ $a_{29} = -0.0034$ $a_{31} = -0.1503$ $a_{36} = 0.265$ $a_{37} = 0.337$ $a_{38} = 0.188$ $a_{39} = 0$ $a_{40} = 0.088$ $a_{41} = -0.196$ $a_{42} = 0.044$

(continued)

**Table 2 (continued)**

Sl no.	Abbreviation of the equation	Standard form of equation	Coefficients value for zero periods
		$f_5 = \begin{cases} a_{10} \ln \left( \frac{V_{s,30}^*}{V_{Lin}} \right) - b \ln \left( \widehat{S}_a + c \right) + b \ln \left[ \widehat{S}_a + c \left( \frac{V_{s,30}^*}{V_{Lin}} \right)^n \right] & V_{s,30} \geq V_{Lin} \\ a_{10} + b_n \left( \frac{V_{s,30}^*}{V_{Lin}} \right) & V_{s,30} < V_{Lin} \end{cases}$	$\begin{aligned} V_{Lin} &= 660 \\ b &= -1.47 \\ n &= 1.5 \\ c &= 2.4 \end{aligned}$
		$V_{s,30}^* = \begin{cases} V_{s,30} & V_{s,30} < V_1 \\ V_1 & V_{s,30} \geq V_1 \end{cases}$	
		$V_1 = \begin{cases} 1500T \leq 0.5s \\ \exp \left[ -0.35 \ln \left( \frac{T}{0.5} \right) + \ln 1500 \right] & 0.5s < T < 3s \\ 800T \geq 3s \end{cases}$	
		$f_4 = a_{13} T_1 T_2 T_3 T_4 T_5$	
		$T_1 = \begin{cases} (90 - dip) / 45 & dip > 30^\circ \\ \frac{60}{45} dip & dip < 30^\circ \end{cases}$	
		$T_2 = \begin{cases} 1 + a_2 HW(M - 6.5)M \geq 6.5 \\ 1 + a_2 HW(M - 6.5) - (1 - a_2 HW)(M - 6.5)^2 & 5.5 < M < 6.5 \\ 0M \leq 6.5 \end{cases}$	
		$T_3 = \begin{cases} h_1 + h_2 (R_x / R_1) + h_3 (R_x / R_1)^2 & R_x < R_1 \\ 1 - \left( \frac{R_x - R_1}{R_2 - R_1} \right) & R_1 \leq R_x < R_2 \\ 0R_x > R_2 \end{cases}$	
		$T_4 = \begin{cases} 1 - \frac{Z_T^2}{100} & Z_{TOR} \leq 10 \text{ km} \\ 0Z_{TOR} > 10 \text{ km} \end{cases}$	

(continued)

**Table 2 (continued)**

Sl no.	Abbreviation of the equation	Standard form of equation	Coefficients value for zero periods
		$T_5 = \begin{cases} 1 - \frac{R_{y0} - R_{y1}}{5} & \text{if } R_{y0} - R_{y1} \leq 0 \\ 0 & \text{if } R_{y0} - R_{y1} < 5 \\ 0 & \text{if } R_{y0} - R_{y1} < 5 \end{cases}$ <p> <math>R_1 = W \cos(dip)</math>  <math>R_2 = 3R_1</math>  <math>R_{y1} = R_x \tan(20)</math>  <math>h_1 = 0.25</math>  <math>h_2 = 1.5</math>  <math>h_3 = -0.75</math>                      If <math>R_{y0}</math> is not available                 </p>	
		$T_5 = \begin{cases} 1 & \text{if } r_{jb} = 0 \\ 1 - \frac{r_{jb}}{30} & \text{if } r_{jb} < 30 \\ 0 & \text{if } r_{jb} \geq 30 \end{cases}$	
		$f_6 = \begin{cases} a_{15} \frac{Z_{TOR}}{30} & \text{if } Z_{TOR} < 20 \text{ km} \\ a_{15} & \text{if } Z_{TOR} \geq 20 \text{ km} \end{cases}$	
		$f_{10} = \begin{cases} a_{43} \ln \left( \frac{Z_1 + 0.01}{Z_{1,ref} + 0.01} \right) & \text{if } V_{s,30} \leq \frac{200 \text{ m}}{s} \\ a_{44} \ln \left( \frac{Z_1 + 0.01}{Z_{1,ref} + 0.01} \right) & \text{if } 200 < V_{s,30} \leq \frac{300 \text{ m}}{s} \\ a_{45} \ln \left( \frac{Z_1 + 0.01}{Z_{1,ref} + 0.01} \right) & \text{if } 300 < V_{s,30} \leq \frac{500 \text{ m}}{s} \\ a_{46} \ln \left( \frac{Z_1 + 0.01}{Z_{1,ref} + 0.01} \right) & \text{if } V_{s,30} > \frac{500 \text{ m}}{s} \end{cases}$	
		$Z_{1,ref} = \begin{cases} \frac{1}{1000} \exp \left[ -\frac{7.15}{4} \ln \left( \frac{V^4_{s,30} + 570.94^4}{1360^4 + 570.94^4} \right) \right] & \text{for California} \\ \frac{1}{1000} \exp \left[ -\frac{5.23}{2} \ln \left( \frac{V^4_{s,30} + 412.39^4}{1360^4 + 412.39^4} \right) \right] & \text{for Japan} \end{cases}$	

(continued)

**Table 2 (continued)**

Sl no.	Abbreviation of the equation	Standard form of equation	Coefficients value for zero periods
		$f_{11} = \begin{cases} a_{14} CR_j b \leq 5 \text{ km} \\ a_{14} \left[ 1 - \frac{CR_j b - 5}{10} \right] 5 < CR_j b \leq 15 \text{ km} \\ 0 CR_j b \geq 15 \text{ km} \end{cases}$ $\text{Regional} = F_{TW}(f_{12} + a_{25}rup) + F_{CN}a_{28}rup + F_{JP}(f_{13} + a_{29}rup)$ $f_{12} = \ln \left( \frac{V_{s,30}^*}{V_{s,30}^{Lin}} \right)$ $f_{13} = \begin{cases} a_{36} V_{s,30} < \frac{200 \text{ m}}{3} \\ a_{37} 200 \leq V_{s,30} < \frac{300 \text{ m}}{3} \\ a_{38} 300 \leq V_{s,30} < \frac{400 \text{ m}}{3} \\ a_{39} 400 \leq V_{s,30} < \frac{500 \text{ m}}{3} \\ a_{40} 500 \leq V_{s,30} < \frac{700 \text{ m}}{3} \\ a_{41} 700 \leq V_{s,30} < 1000 \text{ m/s} \\ a_{42} V_{s,30} \geq 1000 \text{ m/s} \end{cases}$	
		<p>Where, Sa is in g</p> <p><math>\widehat{Sa}</math> is median spectral acceleration in g for reference</p> <p>W is the down-dip rupture width</p>	

(continued)

**Table 2 (continued)**

Sl no.	Abbreviation of the equation	Standard form of equation	Coefficients value for zero periods
12	BA_14	$\ln Y = F_E + F_P + F_S$ $F_E = \begin{cases} e_0 U + e_1 SS + e_2 NS + e_3 RS + e_4 (M_w - M_h) + e_5 (M_w - M_h)^2 M \leq M_h \\ e_0 U + e_1 SS + e_2 NS + e_3 RS + e_6 (M_w - M_h) M > M_h \end{cases}$ $F_P = [c_1 + c_2 (M_w - M_{ref})] \ln(R/R_{ref}) + (c_3 + \Delta c_3)(R - R_{ref})$ $R = \sqrt{r_a^2 + h^2}$ $F_S = \ln(F_{Lin}) + \ln(F_{nl}) + F_{\delta z_1}(\delta z_1)$ $\ln(F_{Lin}) = \begin{cases} \ln\left(\frac{V_{s30}}{V_{ref}}\right) V_{s30} \leq V_c \\ \ln\left(\frac{V_c}{V_{ref}}\right) V_{s30} > V_c \end{cases}$ $\ln(F_{nl}) = f_1 + f_2 \ln\left(\frac{PGA_T + f_3}{f_3}\right)$ $f_2 = f_4 [\exp\{f_5(\min(V_{s30}, 760) - 360)\} - \exp\{f_5(760 - 360)\}]$ $F_{\delta z_1} = \begin{cases} 0T < 0.65 \\ f_6 \delta z_1 T \geq 0.65 \text{ and } \delta z_1 \leq f_7/f_6 \\ f_7 T \leq 0.65 \text{ and } \delta z_1 > f_7/f_6 \end{cases}$ $\delta z_1 = z_1 - \mu z_1$ $\ln \mu z_1 = \begin{cases} -\frac{7.15}{4} \ln\left(\frac{V_{s30}^4 + 570.94^4}{1360^4 + 570.94^4}\right) \text{ for California} \\ -\frac{5.23}{2} \ln\left(\frac{V_{s30}^4 + 412.39^4}{1360^4 + 412.39^4}\right) \text{ for Japan} \end{cases}$	$M_{ref} = 4.5$ $R_{ref} = 1 \text{ km}$ $V_{ref} = 760 \text{ m/s}$ $e_0 = 0.4473$ $e_1 = 0.4856$ $e_2 = 0.2459$ $e_3 = 0.4539$ $e_4 = 1.4310$ $e_5 = 0.05053$ $e_6 = -0.1662$ $M_h = 5.5$ $c_1 = -1.134$ $c_2 = 0.1917$ $c_3 = -0.008088$ $\Delta c_3$ , China, Turkey = 0.0028576 $\Delta c_3$ , Italy, Japan = -0.00255 $h = 4.5$ $c = -0.6$ $V_c = 1500 \text{ m/s}$ $f_1 = 0$ $f_3 = 0.1$ $f_4 = -0.15$ $f_5 = -0.00701$ $f_6 = -9.9$ $f_7 = -9.9$

Where, Y is in g  
 PGA<sub>T</sub> is median PGA for reference rock (i.e., V<sub>s30</sub> = V<sub>ref</sub>)  
 If strike slip faulting mechanism, then SS = 1  
 If Normal faulting mechanism, then NS = 1  
 If Reverse faulting mechanism, then RS = 1  
 If unspecified faulting mechanism, then U = 1

where,  $w_{unif} = 1/M$ ,  $M$  is the number of models used for the calculation of LLH. Positive DSI indicates the GMPE supports the observed model, whereas negative DSI rejects the GMPE model. This LLH, weight, and DSI are further used to select and weight the GMPEs for the hazard estimation of the Himalayan region. In the present study, an efficacy test has been carried out by considering the macroseismic intensity maps of 1897 Shillong (8.0  $M_w$ ), 1934 Bihar–Nepal (8.0  $M_w$ ), 1991 Uttarkashi (6.8  $M_w$ ), 2005 Kashmir (7.6  $M_w$ ), and 2015 Nepal (7.8  $M_w$ ) earthquakes. The intensity map is converted to a PGA map using the PGA-Intensity equations proposed by Anbazhagan et al. (2016b). Using these derived PGA values, LLH values (Eq. (3)) and corresponding weights (Eq. (4)) have been calculated. Observing the applicability and trends in GMPEs, the hypocentral distance is divided into three distance bins 0–100 km, 100–300 km, and more than 300 km. As five different intensity maps are used for ranking of GMPEs and each one of them has a different ranking, commoning these derived PGA values, GMPdEs are selected for different distance bins, and average weights are assigned to the GMPEs. The selected GMPEs, along with the weight for different distance bins, are given in Table 3. The weight factor corresponding to particular GMPE for different distance bins is further used to evaluate the seismic hazard values in terms of PGA and SA.

**Table 3** Weights and Ranking of GMPE for different distance bins used in hazard analysis of the IGB

GMPE	Weight	Ranking
<i>Distance ≤ 100 km</i>		
BAN_19	0.28	1
ID_14	0.22	2
ZH_06	0.16	3
AN_13	0.14	4
NA_09	0.10	5
CABO_14	0.10	6
<i>100 km &lt; Distance ≤ 300 km</i>		
BAN_19	0.28	1
ID_14	0.20	2
BA_14	0.17	3
ZH_16_CM	0.15	4
KA_06	0.10	5
CABO_14	0.10	6
<i>Distance &gt; 300 km</i>		
BAN_19	0.65	1
NDMA_10	0.35	2

## 5 The Shape of Design Spectrum for HR

SHA analysis gives hazard values in PGA and SA at different periods, but these cannot be used directly in the design, as the design spectrum is a normalized and smoothed spectrum. The normalized and smoothed design spectrum reflects the median value of several response spectra with acceleration, velocity, and displacement sensitive zone based on regional recorded earthquake data. In the sixth revision of Indian seismic code BIS:1893 (BIS. IS, 2016), two design spectra were given for equivalent static and response spectra for constructing the acceleration response spectra. The typical design spectra given in BIS:1893 (BIS. IS, 2016) are considered in the present study for comparison. Normalized and smoothed design spectra were introduced in the Indian code 2002 version. In older versions of Indian code, BIS 1893 up to revision 3, 1970, design acceleration is given as average acceleration in  $\text{cm}/\text{sec}^2$  and 5% damping maximum average acceleration of  $190 \text{ cm}/\text{s}^2$  (0.28 g) at 0.3 s of the natural period of the structure. In 1984, this was converted as an average acceleration coefficient ( $S_a/g$ ), and the shape of the design spectrum started here. BIS1893 (BIS. IS, 2016) version  $S_a/g$  linear slope up to 0.12 s, the maximum value of 0.28 from 0.12 to 0.33 s constant value and beyond 0.33 s reduced up to 3.0 s of the natural period of vibration of 5% damping. The first normalized and smoothed design spectrum was introduced in the BIS1893 (BIS IS 2002) version with three major types of ground (rock/hard soil/ medium soil and soft soil). The average acceleration coefficient is replaced by the spectral acceleration coefficient ( $S_a/g$ ), and the natural period of vibration is replaced with a period (natural period of structure). Minimum  $S_a/g$  at 0 s, linearly increases  $S_a/g$  up to 0.1 s and reaches  $S_a/g$  of 2.5 and remains constant  $S_a/g$  of 2.5 from 0.1 to 0.4 s then  $S_a/g$  decreases non-linearly 0.4–4.0 s of the period. One more normalized and smoothed design spectrum is added in the BIS1893 (BIS. IS, 2016) version with the initial part  $S_a/g$  being 2.5 from 0 to 0.4 s for the equivalent static design method. As per the author's knowledge, very limited regional seismic data and analysis went into the shape of the present design spectrum in IS 1893 (BIS. IS, 2016). It may be an appropriate time to arrive at a normalized and smoothed design spectrum considering rock earthquake records available.

### 5.1 Design Spectrum for Code

In most seismic designs, the estimation of the seismic force of a typical structure is based on the 5% damped design response spectrum. Generally, a given site's design spectrum is obtained by modifying the normalized and smoothed spectrum by considering site factors corresponding to a seismic site class. Conventionally, the design force is specified using response spectrum amplitude. However, with the increased complexity of the modern structure and understanding, the structure's seismic performance is in high demand in seismic prone areas. So, it is necessary to specify the amplitude and shape of the design spectra considering regional parameters.

Initially, Biot (1941) introduced a response spectra concept and proposed the standard spectral shape for earthquake resistant design of a building. Housner () averaged and smoothed the response spectra considering the four strong-motion records and proposed using average spectrum shape in earthquake engineering design. Newmark and Hall (1969, 1982) recommended a smooth response spectrum concentrating on three regions viz. acceleration (short period), velocity (medium period), and displacement (long period). These three spectral regions can be constructed by applying the amplification to the design value of PGA, peak ground velocity (PGV), and peak ground displacement (PGD). The spectral acceleration for periods  $<0.33$  s, between  $0.33$  and  $3.33$  s and above  $3.33$  s, is sensitive to PGA, PGV, and PGD, respectively (Newmark & Hall, 1982). In most engineering practices, Housner and Newmark spectra's fixed shape, normalized to unit peak acceleration, is widely used by scaling it based on the design peak acceleration. Various researchers (Hall et al., 1975; Mohraz, 1976) contributed to the development of the Newmark–Hall spectrum. The response spectra can also be presented using the tripartite plot or four-way logarithmic plot for which all the spectra quantities can be read. This tripartite plot is the compact representation of three response spectra. So, in this study, we arrive at the shape and three regions, viz. acceleration, velocity, and displacement of HR, using data discussed in Sect. 2.

## 5.2 *Spectrum Control Period and Factor*

Malhotra (2001) finds that the response of the structure derived using acceleration time history does not correspond to the velocity and displacement time histories. The response of the flexible structures (long period) can be contradictory if computed only using processed acceleration time history (Malhotra 2001). Based on that, Malhotra (2001) proposed a methodology to compute elastic response spectra for incompatible acceleration, velocity, and displacement time histories. Using the acceleration, velocity, and displacement time histories, Malhotra (2006) determined the amplification factors for the spectrum's acceleration, velocity, and displacement sensitive region for various damping values. We followed the procedure recommended by Malhotra (2001, 2009) for deriving the normalized response spectra by adopting an in-house MATLAB code developed by the Authors.

Various authors (Malhotra, 2006; Mohraz et al., 1972; Newmark & Hall, 1982) defined the different cutoff period of the design spectrum that is sensitive to PGA, PGV, and PGD. Newmark and Hall (1982) and Mohraz et al. (1972) assumed that SAs for periods  $0.33$  s,  $0.33$  and  $3.33$  s, and more than  $3.33$  s are sensitive to PGA, PGV, and PGD. SAs for the periods up to  $0.62$ ,  $0.62$ – $2.6$  s, and the rest correlated well with PGA, PGV, and PGD (Malhotra, 2006). Malhotra (2006) concluded that cutoff periods could change for different sets of seismic ground motions, and also, it was concluded that vertical response spectra do not have the same shape as the horizontal spectra. The recorded bedrock seismic ground motion data in the HR has been used to determine the cutoff periods for PGA, PGV, and PGD sensitive regions. The PGA,

PGV, and PGD sensitive region for HR has been defined by correlating SA at various periods with PGA, PGV, and PGD in a plot (Fig. 4). From Fig. 4, it can be noted that in the region, SA for the period up to 0.38 s is correlating well with PGA, the period between 0.38 and 2.33 s, and SA is correlating well with PGV, and the rest correlate best with PGD for the rock sites. Bureau of Indian Standard (BIS. IS, 2016) defined the cutoff period for rock sites as 0.1 and 0.4 s, which is significantly different from the present study. Similarly, it is noted here that the cutoff period calculated in this study is considerably different from Hall et al. (1982).

All recorded earthquake acceleration time history of engineering interest ( $PGA > 0.01 \text{ g}$ ) is further plotted in a tripartite plot and shown in Fig. 5. The spectral velocity (SV) is converted from the spectral displacement. Also, the average of the seismic ground motions has been normalized using Eqs. (6)–(8). Firstly, the central period ( $T_{cg}$ ) of the seismic ground motion is calculated as

$$T_{cg} = 2\pi \sqrt{\frac{PGD}{PGA}} \tag{6}$$

This  $T_{cg}$  caused the horizontal shift in the response spectra, PGA and PGD change to  $PGA \times T_{cg}/2\pi$  and  $PGD \times 2\pi/T_{cg}$  respectively; however, PGV remains constant. Further, PGV and SV are normalized with respect to  $\sqrt{PGA \cdots PGD}$ , this makes PGA and PGD unity, and PGV and SV to take the following non-dimensional form

$$\overline{PGV} = \frac{PGV}{\sqrt{PGA \cdots PGD}} \tag{7}$$

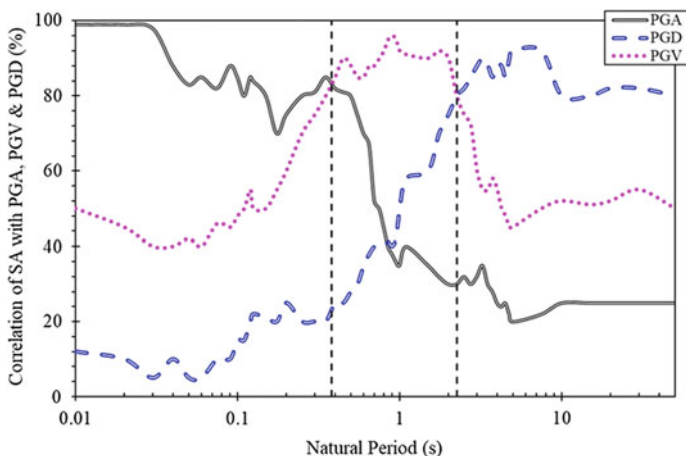


**Fig. 4** Correlation of SA at various periods with PGA, PGV, and PGD for the Himalayan Region at bedrock condition

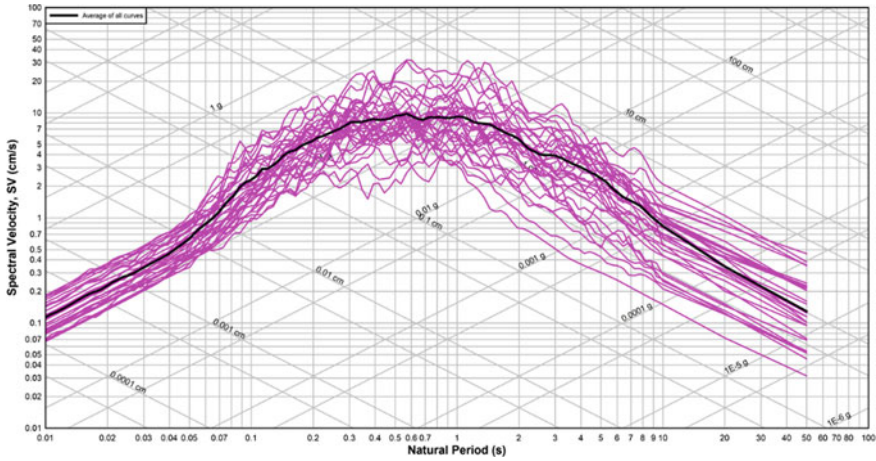


**Fig. 5** A tripartite plot of horizontal seismic ground motions recorded at bedrock in the Himalayan region

$$\overline{SV} = \frac{SV}{\sqrt{PGA \cdots PGD}} \tag{8}$$

Further, the normalized spectrum has been smoothed, considering the least-squares fitting of straight-line segments through the median curve. The median normalized spectrum is further obtained by averaging the  $\log \overline{SA}$  at each normalized period. The median normalized spectrum versus the normalized spectral period is given in Figure 6a for the Himalayan region. The shaded area in Fig. 6a corresponds to  $\pm 1$  standard deviation about the median. The smooth response spectrum has been obtained afterwards by using the least-squares fitting of straight-line segments through the median curve as shown in Fig. 6b. Figure 6b shows the smooth medium spectrum of HR. The Himalayan region multiplication factors for PGA, PGV, and PGD are 2.29, 1.97, and 2.05 respectively and denoted as  $\alpha_A$ ,  $\alpha_V$ , and  $\alpha_D$ . In Fig. 6b, we can also note the control periods for constant acceleration is 0.15 s, velocity is 0.38 s, and displacement is 2.33 s, respectively, for the region. These values are also comparable with Fig. 4.

### 5.3 Bedrock Horizontal Design Spectrum for Himalayan Region

The shape of the design spectrum at bedrock in the region depends on smoothed and normalized response spectra for acceleration, velocity and displacement-control period. In the previous section, we find that the control periods of HR based on the

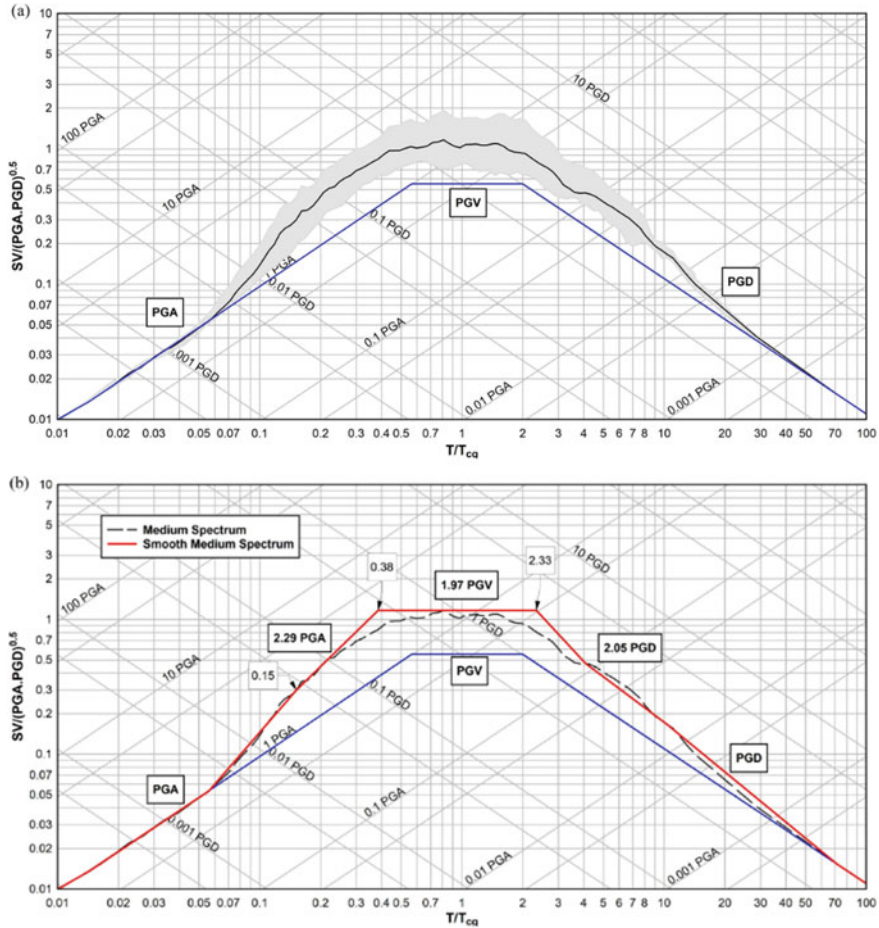


**Fig. 6** Himalayan region **a** Normalized 5% damping median spectrum of horizontal seismic ground motions recorded data at bedrock and **b** smooth medium spectrum

recorded data for acceleration is 0.15 s ( $T_B$ ), velocity is 0.38 s ( $T_C$ ), and displacement is 2.33 s ( $T_D$ ). Similarly, modification factors of  $\alpha_A$ ,  $\alpha_V$ , and  $\alpha_D$  as 2.29, 1.97, and 2.05. These factors control the shape of the Horizontal Design Spectrum (HDS) in the region. The spectral shape is a composite of the very low period branch from PGA to the constant acceleration i.e., up to 0.15 s ( $T_B$ ), constant acceleration branch in between 0.15 and 0.38 s, velocity branch from 0.38 to 2.33 s, and displacement branch beyond 2.33 s. The peak of the spectral amplitude is defined as  $2.5 \eta S$ , where  $\eta$  is the damping ratio i.e., 5% (CEN 2005). The general form of equations for the elastic response spectra for 5% damping is as

$$0 \leq T \leq T_B: \frac{S_a(T)}{PGA_{rock}} = s \cdot \left[ 1 + \frac{T}{T_B} \cdot (\beta - 1) \right] \tag{9}$$

$$T_B \leq T \leq T_C: \frac{S_a(T)}{PGA_{rock}} = s \cdot \beta \tag{10}$$

$$T_C \leq T \leq T_D: \frac{S_a(T)}{PGA_{rock}} = s \cdot \beta \cdot \frac{T_C}{T} \tag{11}$$

$$T_D \leq T: \frac{S_a(T)}{PGA_{rock}} = s \cdot \beta \cdot T_C \frac{T_D}{T^2} \tag{12}$$

Here,  $PGA_{rock}$  is the design ground acceleration at rock site conditions,  $S$  and  $\beta$  are the soil amplification here it is unity as all sites are rock stations and spectral amplification factors.  $T_B$  and  $T_C$  are the limits of constant acceleration branch and  $T_D$  is the beginning of the constant displacement range of the spectrum. The parameters  $S$ ,  $\beta$ ,  $T_B$ ,  $T_C$ , and  $T_D$  depend on on-site class and seismicity. In the present study, these parameters are derived based on recorded seismic data from India’s Himalayan region, as discussed in the previous sections. Figure 7 shows the normalized and smoothed spectrum developed for the study area. The shape of the design spectrum from the study is different from IS 1893 (BIS, IS, 2016). The design spectrum for the typical PGA value of 0.24 g and 0.36 g has been generated for the shape obtained in this study and shown in Fig. 8. It can be noted that the design spectrum developed in this is sensitive to the size of an earthquake, similar to modern seismic codes. But BIS

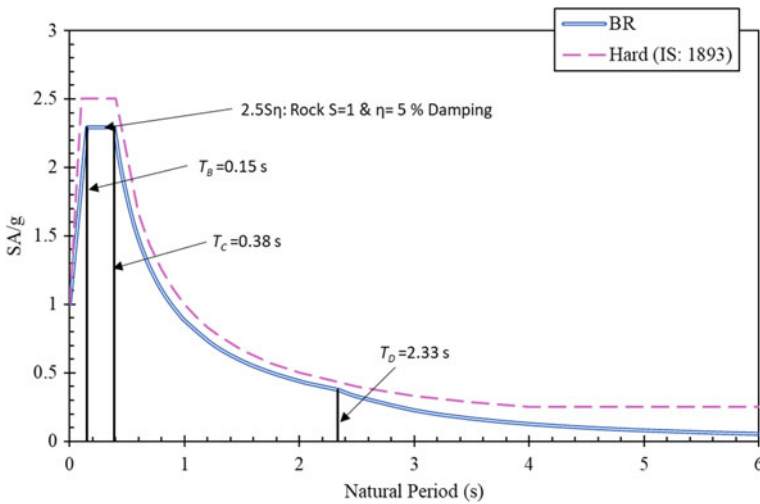
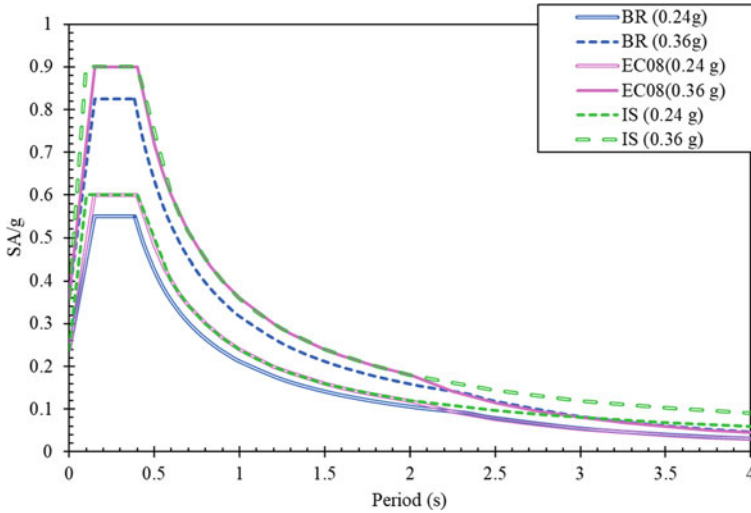


Fig. 7 Normalized and smoothed horizontal design spectrum for Himalayan region



**Fig. 8** Typical design spectrum for the region considering PGA value of 0.24 g and 0.36 g

code spectrum does not change with PGA values, and the design spectrum is the function of the period i.e.,  $T$  rather than PGA,  $S$ ,  $\beta$ , and variation of  $T$ . Proposed spectrum for HDR for 5% damping and other damping values region-specific damping values given by Anbazhagan et al. (2016a) can be used. Similar way, we are also working on a vertical design spectrum based on available data and trying to understand how is the ratio of horizontal to vertical spectrum in the region.

From Fig. 8, we note that IS code design spectrum closely matched with Euro code rather Indian data derived design spectrum. As everyone knows, that design spectrum given in IS 1893 initial version of code was taken from the design spectrum arrived based on western recorded earthquake data. The design spectrum was repeatedly reused in all revisions of IS 1893 without developing a new spectrum based on Indian recorded data. The new design spectrum derived in this study using Indian data has a considerable difference from the Euro/India code, which may be due to changes in seismicity and seismotectonic of both regions. Presently we used all available data from the Himalayan region as one group, but it can also be highlighted that HR can be grouped into three major seismic areas (Western, Central and Eastern Part) based on seismicity and seismotectonic. This spectrum may be updated when more record earthquake data are available from each region. Further, soil layers and their thickness variation in each site can amplify bedrock ground motions. Such kind of amplified ground motions cause catastrophic damage during past earthquakes in HR. The understating and estimating design spectrum for different soil classes are also required.

## 6 Soil Amplification and Spectrum

Many highly populated cities are located in IGB, which is very close to the Himalayan region. IGB experienced catastrophic damages due to geo-seismic hazards of site amplification and liquefaction during past earthquakes. Limited study has been carried out to understand site amplification considering site-specific soil and seismicity data and dynamic models of shear modulus reduction and damping ratio curves. We made an extensive study to understand the subsurface dynamic properties of IGB. Bajaj and Anbazhagan (2019) carried out the combined active and passive MASW (Multichannel Analysis of Surface Wave) survey at 275 locations, and the shear wave velocity is measured up to a depth of 500 m. The entire IGB was classified based on the average shear wave velocity map at shallow as well as deeper depths. The average shear wave velocity till top 5, 10, 15, 20, 30, 50, 100, 150, 200, 250, and 300 m depths was estimated and mapped. The shear wave velocity near the upper Ganga plain is  $215 \pm 20$  m/s till 10 m depth and increases to  $750 \pm 50$  m/s till 150 m depth, which is due to the thick deposits of Varanasi older alluvium. Further, we mapped the depth of the non/less-amplifying layer in IGB, i.e., depth of layer having  $V_s \geq 1500$  m/s. Further, the spatial variation of depth at which shear wave velocity is equal/more than 1500 m/s is also studied. Figure 9 shows thickness from surface layer up to layer with  $V_s \geq 1500$  m/s from our study. It can be noted that for the whole IGB,  $V_s$  more than 1500 m/s is observed at different depths, and this may be due to the variation in a deposition in different geological eras. Varying soil stiffness ( $V_s$  values) in the vertical and horizontal direction of the IGB may be

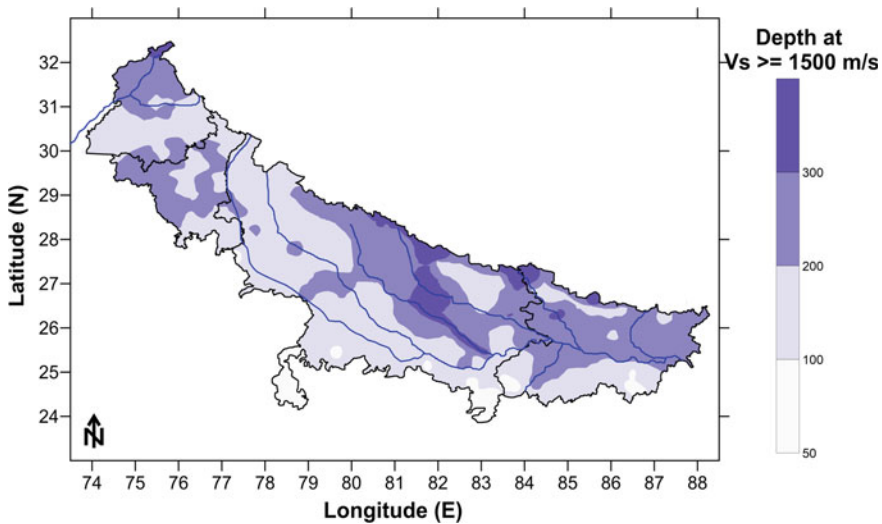


Fig. 9 Depth of amplifiable soil layers in IGB

one of the reasons for past heavy damages due to earthquake geohazards in the IGB (2020). So, the authors highlighted the importance of understating site effects, and liquefaction may be of prime importance to reduce seismic-related losses.

Most amplification studies do not fully account for regional soil and seismic parameters to spell out representative amplification in IGB. Bajaj and Anbazhagan (2019a) used the above study results and generated time average shear wave velocity at 30 m depth ( $V_{S30}$ ), which is an essential parameter for site characterization and site amplification estimation by an empirical approach. But empirical formulas developed for the different regions should be used with caution. Bajaj and Anbazhagan (2020) produced representative amplification by carrying out a non-linear site response analysis at 275 locations by assigning suitable input motion based on a seismic hazard map for a 10% probability of exceedance in 50 years. The study found the amplification factor in Punjab-Haryana as 2.8–3.9, Uttar Pradesh as 1.5–3.4, and Bihar region as 1.8–6.3. Reliable soil and seismic input parameters were used in the study, but dynamic soil models were assigned from the parametric study by Bajaj and Anbazhagan (2020) for Japan Kiki net soil and earthquake data. IGB is more prone to local site effects due to varying predominant frequency and thickness of soil column (Anbazhagan et al., 2019). So reliable amplification factor estimation and development of HDS for different site classifications in IGB and HR are required to reduce seismic-related damages in north India.

## 7 Summary and Conclusion

First time compressive regional available earthquake recorded data at rock sites from the Himalayan region was presented here. These data are used to identify GMPE functional form and suggest a list of suitable GMPEs for seismic hazard analysis. The study found that many of the GMPEs developed in the region do not follow the proper attenuation functional form suitable for the Himalayan region. Detailed LLH analysis was carried out considering applicable GMPEs using regional ground motion data. The most suitable GMPEs for SHA has ranked with weight calculation for the logic tree probabilistic calculation. The most ranked Indian GMPEs in all distance segments are proposed by Bajaj and Anbazhagan (2019b). We also arrived design spectrum shape for the rock site first time for HR using recorded data. We found that controlled periods and the highest  $Sa/g$  are different from the current BIS 1893 code. This needs to be taken into account while designing structures in the region. There is no systematic amplification estimation found in the area, even though many soil and seismic ground motion data are available. This needs to be addressed in future studies, and some of them are in progress in our research team.

**Acknowledgements** The authors are thankful for funding and support by the Science and Engineering Research Board (SERB), Department of Science and Technology [SERB/F/162/2015-2016]. Author thanks M/s. SECON Private Limited, Bangalore for funding project “Effect of Shear Wave Velocity Calibration on Amplification of Shallow and Deep Soil Sites.”

## References

- Abrahamson, N. A., & Litehiser, J. J. (1989). Attenuation of vertical peak accelerations. *Bulletin of the Seismological Society of America*, 79, 549–580.
- Abrahamson, N., & Silva, W. (2008). Summary of the Abrahamson & Silva NGA ground-motion relations. *Earthquake Spectra*, 24, 67–97.
- Abrahamson, N. A., Silva, W. J., & Kamai, R. (2014). Summary of the ASK14 ground-motion relation for active crustal regions. *Earthquake Spectra*. <https://doi.org/10.1193/070913EQS198M>.
- Aghabarati, H., & Tehranizadeh, M. (2009). Near-source ground motion attenuation relationship for PGA and PSA of vertical and horizontal components. *Bulletin of Earthquake Engineering*, 7, 609–635.
- Akkar, S., & Bommer, J. J. (2010). Empirical equations for the prediction of PGA, PGV and spectral acceleration in Europe, the Mediterranean region and the Middle East. *Seismological Research Letters*, 81, 195–206.
- Akkar, S., Sandikkaya, M. A., & Bommer, J. J. (2014). Empirical ground motion models for point and extended-source crustal earthquake scenarios in Europe and the Middle East. *Seismological Research Letters*, 12, 359–387.
- Ambraseys, N., Douglas, J. S., Sarma, K., & Smit, P. M. (2005). Equation for the estimation of strong ground motions from shallow crustal earthquakes using data from Europe and the Middle East: Horizontal peak ground acceleration and the spectral acceleration. *Bulletin of Earthquake Engineering*, 3, 1–53.
- Anbazhagan, P., Kumar, A., & Sitharam, T. G. (2013). Ground motion prediction equation considering combined dataset of recorded and simulated ground motions. *Soil Dynamics and Earthquake Engineering*, 53, 92–108.
- Anbazhagan, P., Bajaj, K., & Patel, S. (2015). Seismic hazard maps and spectrum for Patna considering region-specific seismotectonic parameters. *Natural Hazards*, 78(2), 1163–1195.
- Anbazhagan, P., Uday, A., Moustafa, S. S. R., & Al-Arifi, N. S. N. (2016a). Pseudo-spectral damping reduction factors for the himalayan region considering recorded ground-motion data. *Plos One*, 11(9), e0161137.
- Anbazhagan, P., Bajaj, K., Moustafa, S. S. R., & Al-Arifi, N. S. N. (2016b). Relationship between intensity and recorded ground motion and spectral parameters for the Himalayan region. *Bulletin of the Seismological Society of America*, 106(4), pp. 1672–1689.
- Anbazhagan, P., Janarthan, B., & Shaivan, H. S. (2019a). Empirical correlation between sediment thickness and resonant frequency using HVSR for the Indo-Gangetic Plain. *Current Science*, 117(9), 1182–1491.
- Anbazhagan, P., Srilakshmi, K. N., Bajaj, K., Moustafa, S. S. R., & Al-Arifi, N. S. N. (2019b). Determination of Seismic site classification of seismic recording stations in the Himalayan region using HVSR method. *Soil Dynamics and Earthquake Engineering*, 116, 304–316.
- Anbazhagan, P., Bajaj, K., Matharu, K., Moustafa, S. S. R., & Al-Arifi, N. S. N. (2019c). Probabilistic seismic hazard analysis using the logic tree approach—Patna district (India). *Natural Hazards and Earth System Sciences*, 19(10), 2097–2115. <https://doi.org/10.5194/nhess-19-2097-2019>.
- Atkinson, G. M., & Boore, D. M. (2003). Empirical ground-motion relations for subduction-zone earthquakes and their applications to Cascadian and other regions. *Bulletin of the Seismological Society of America*, 93, 1703–1717.
- Bajaj, K., & Anbazhagan, P. (2018). A comparison of different functional form and modification of NGA-West 2 Ground-Motion Prediction Equation for the Himalayan region. *Journal of Seismology*, 22(1), 161–185.
- Bajaj, K., & Anbazhagan, P. (2019a). Seismic site classification and correlation between Vs and SPT-N for deep soil sites in Indo-Gangetic Basin. *Journal of Applied Geophysics*, 163, 55–72.
- Bajaj, K., & Anbazhagan, P. (2019b). Regional seismological model parameter estimation and development of GMPE model for the active region of Himalaya. *Soil Dynamics and Earthquake Engineering*, 126, 105825.

- Bajaj, K., & Anbazhagan, P. (2020). Comprehensive amplification estimation of the Indo Gangetic Basin deep soil sites in the seismically active area. *Soil Dynamics and Earthquake Engineering*, *127*, 105855.
- Bajaj, K., & Anbazhagan, P. (2021a). Detailed seismic hazard, disaggregation and sensitivity analysis for Indo Gangetic basin. *Pure and Applied Geophysics*, *178*, 1977–1999.
- Bajaj, K., & Anbazhagan, P. (2021b) Identification of shear modulus reduction and damping curve for deep and shallow sites: Kik-Net data. *Journal of Earthquake Engineering*. Published Online: <https://doi.org/10.1080/13632469.2019.1643807>.
- Bilham, R. (2015). Raising Kathmandu. *Nature Geoscience*, *8*, 582–584.
- Bindi, D., Massa, M., Luzi, L., Ameri, G., Pacor, F., Puglia, R., & Augliera, P. (2014). Pan-European ground motion prediction equations for the average horizontal component of PGA, PGV, and 5%-damped PSA at spectral periods up to 3.0 S using the RESOURCE dataset. *Bulletin of Earthquake Engineering*, *12*, 391–430.
- Biot, M. A. (1941). A mechanical analyzer for the prediction of earthquake stresses. *Bulletin of the Seismological Society of America*, *31*, 151–71.
- BIS IS 1893–2002 (Part 1): Indian standard criteria for earthquake resistant design of structures. Part 1—General provisions and buildings. Bureau of Indian Standards, New Delhi.
- BIS. (2016). IS 1893–2016 (Part 1): Indian standard criteria for earthquake resistant design of structures. Part 1—General provisions and buildings. Bureau of Indian Standards, New Delhi.
- Bommer, J. J., Douglas, J., Scherbaum, F., Cotton, F., & Bungum, H., & Fäh, D. (2010). On the selection of ground-motion prediction equations for seismic hazard analysis. *Seismological Research Letters*, *81*(5), 783–793.
- Boore, D. M., & Bommer, J. (2005). Processing of strong motion accelerograms: Needs, options and consequences. *Soil Dynamics and Earthquake Engineering*, *25*, 93–115.
- Boore, D. M., & Atkinson, G. M. (2008). Ground-motion prediction equations for the average horizontal component of PGA, PGV and 5% damped PSA at spectral periods between 0.01 and 10.0 s. *Earthq Spectra*, *24*(1), 99–138.
- Boore, D. M., Stewart, J. P., Seyhan, E., & Atkinson, G. M. (2014). NGAWest 2 equations for predicting PGA, PGV, and 5%-damped PSA for shallow crustal earthquakes. *Earthquake Spectra*, *30*(3), 1057–1085.
- Campbell, K. W. (1997). Empirical near-source attenuation relationships for horizontal and vertical components of peak ground acceleration, peak ground velocity and pseudo-absolute acceleration response spectra. *Seismological Research Letters*, *68*(1), 154–179.
- Campbell, K. W., & Bozorgnia, Y. (2008). NGA ground motion model for the geometric mean horizontal component of PGA, PGV, PGD and 5 % damped linear elastic response spectra for period ranging from 0.01 to 10 s. *Earthquake Spectra*, *24*, 139–171.
- Campbell, K. W., & Bozorgnia, Y. (2014). NGA-West 2 ground motion model for the average horizontal components of PGA, PGV, and 5%-damped linear acceleration response spectra. *Earthquake Spectra*, *30*(3), 1087–1115.
- Cauzzi, C., & Faccioli, E. (2008). Broadband (0.05 to 20s) prediction of displacement response spectra based on worldwide digital records. *Journal of Seismology*, *12*(4), 453–475.
- CEN (2005) EN 1998-3 Eurocode 8: design of structures for earthquake resistance, part 3: assessment and retrofitting of buildings. European Committee for Standardization.
- Chiou, B. S. J., & Youngs, R. R. (2008). An NGA model for the average horizontal component of peak ground motion and response spectra. *Earthquake Spectra*, *24*(1), 173–215.
- Chiou, B. S. J., & Youngs, R. R. (2014). Update of the Chiou and Youngs NGA model for the average horizontal component of peak ground motion and response spectra. *Earthquake Spectra*, *30*, 1117–1153.
- Cotton, F., Scherbaum, F., Bommer, J. J., & Bungum, H. (2006). Criteria for selecting and adjusting ground-motion models for specific target regions: Application to central Europe and rock sites. *Journal of Seismology*, *10*(2), 137–156.
- Das, S., Gupta, I. D., & Gupta, V. K. (2006). A probabilistic seismic hazard analysis of Northeast India. *Earthquake Spectra*, *22*, 1–27.

- Delavaud, E., Scherbaum, F., Kuehn, N., & Allen, T. (2012). Testing the global applicability of ground-motion prediction equations for active shallow crustal regions. *Bulletin of the Seismological Society of America*, 102(2), 702–721.
- Delavaud, E., Scherbaum, F., Kuehn, N., & Riggelsen, C. (2009). Information-theoretic selection of ground-motion prediction equations for seismic hazard analysis: An applicability study using Californian data. *Bulletin of the Seismological Society of America*, 99, 3248–3263.
- Douglus, J (2020). *Ground motion prediction equations 1964–2020*. <http://www.gmpe.org.uk/gmp-report2014.html>.
- Gupta, I. D. (2010). Response spectral attenuation relations for inslab earthquakes in Indo-Burmese subduction zone. *Soil Dynamics and Earthquake Engineering*, 30, 368–377.
- Hall, W. J., Mohraz, B., & Newmark, N. M. (1975). Statistical studies of vertical and horizontal earthquake spectra. Nathan M. Newmark Consulting Engineering Services, Urbana, Illinois.
- Housner, G. W. (1959). Behavior of structures during earthquakes. *Journal of Engineering Mechanics Division, ASCE*, 85(EM 4), 109–29.
- Housner, G. W. (1970). *Design spectrum, Chapter 5 in earthquake engineering*. New Jersey: R.L Wiegel: Prentice-Hall.
- Idriss, I. M. (2008). An NGA empirical model for estimating the horizontal spectral values generated by shallow crustal earthquakes. *Earthquake Spectra*, 16, 363–372.
- Idriss, I. M. (2014). An NGA-West 2 empirical model for estimating the horizontal spectral values generated by shallow crustal earthquakes. *Earthquake Spectra*. <https://doi.org/10.1193/070613EQS195M>
- Iyengar, R. N., & Ghosh, S. (2004). Microzonation of earthquake hazard in Greater Delhi area. *Current Science*, 87(9), 1193–1202.
- Kanno, T., Narita, A., Morikawa, N., Fujiwara, H., & Fukushima, Y. (2006). A new attenuation relation for strong ground motion in Japan based on recorded data. *Bulletin of the Seismological Society of America*, 96, 879–897.
- Kumar, A., Mittal, H., Sachdeva, R., & Kumar, A. (2012). Indian strong motion instrumentation network. *Seismological Research Letters*, 83, 59–66.
- Lin, P. S., & Lee, C. H. (2008). Ground-motion attenuation relationship for subduction-zone earthquakes in Northeastern Taiwan. *Bulletin of the Seismological Society of America*, 98(1), 220–240.
- Malhotra, P. K. (2001) Response spectrum of incompatible acceleration, velocity and displacement histories. *Earthquake Engineering and Structural Dynamics*, 30(2), 279–286.
- Malhotra, P. K. (2006). Smooth spectra of horizontal and vertical ground motions. *Bulletin of the Seismological Society of America*, 96(2), 506–518.
- Mohraz, B. (1976). A study of earthquake response spectra for different geological conditions. *Bulletin of the Seismological Society of America*, 66(3), 915–935.
- Mohraz, B., Hall, W. J., & Newmark, N. M. (1972) A study of vertical and horizontal earthquake spectra, AEC Report WASH-1255, Nathan M. Newmark Consulting Engineering Services, Urbana, Illinois.
- Motazedian, D., & Atkinson, G. M. (2005). Stochastic finite-fault modeling based on a dynamic corner frequency. *Bulletin of the Seismological Society of America*, 95, 995–1010.
- Nath, S. K., Vyas, M., Pal, I., & Sengupta, P. (2005). A hazard scenario in the Sikkim Himalaya from seismotectonics spectral amplification source parameterization and spectral attenuation laws using strong motion seismometry. *Journal of Geophysical Research*, 110, 1–24.
- Nath, S. K., Raj, A., Thingbaijam, K. K. S., Kumar, A. (2009). Ground motion synthesis and seismic scenario in Guwahati city: A stochastic approach *Seismological Research Letters*, 80(2), 233–42.
- NDMA. (2011). *Development of probabilistic hazard map of India*. Retrieved July 2017, from <http://ndma.gov.in/ndma/disaster/earthquake/PSHATechReportMarch%202011.pdf>. Report.
- Newmark, N. M., & Hall, W. J. (1969). Seismic design criteria for nuclear reactor facilities. In *Proceedings of World Conference on Earthquake Engineering*, 4th Santiago, Chile, B-4 (pp. 37–50).

- Newmark, N. M., & Hall, W. J. (1982). *Earthquake spectra and design*. Earthquake Engineering Research Institute, Oakland, California.
- Ramkrishnan, R., Sreevalsa, K., & Sitharam, T. G. (2020) Strong motion data based regional ground motion prediction equations for North East India based on non-linear regression models. *Journal of Earthquake Engineering*. <https://doi.org/10.1080/13632469.2020.1778586>.
- Scherbaum, F., Delavaud, E., & Riggelsen, C. (2009). Model selection in seismic hazard analysis: an information theoretic perspective. *Bulletin of the Seismological Society of America*, 99, 3234–3247.
- Sharma, M. L., & Bungum, H. (2006). New strong ground motion spectral acceleration relation for the Himalayan region. In *First European Conference on Earthquake Engineering and Seismology* (p. 1459).
- Sharma, M. L., Douglas, J., Bungum, H., & Kotadia, J. (2009). Ground-motion prediction equations based on data from Himalayan and Zagros regions. *Journal of Earthquake Engineering*, 13, 1191–1210.
- Singh, R. P., Aman, A., & Prasad, Y. J. J. (1996). Attenuation relations for strong ground motion in the Himalayan region. *Pure and Applied Geophysics*, 147, 161–180.
- Spudich, P., Joyner, W. B., Lindh, A. G., Boore, D. M., Margaris, B. M., & Fletcher, J. B. (1999). SEA99: a revised ground motion prediction relation for use in Extensional tectonic regions. *Bulletin Seismological Society of America*, 89(5), 1156–1170.
- Srivastava, H. N., Verma, M., Bansal, B. K., & Sutar, A. K. (2015). Discriminatory characteristics of seismic gaps in Himalaya. <https://doi.org/10.1080/19475705.2013.839483>.
- Strasser, F. O., Abrahamson, N. A., & Bommer, J. J. (2009). Sigma: Issues, insights, and challenges. *Seismological Research Letters*, 80, 41–56.
- Takahashi, T., Saiki, T., Okada, H., Irikura, K., Zhao, J. X., Zhang, J., Thoi, H. K., Somerville, P. G., Fukushima, Y., & Fukushima, Y. (2004). Attenuation models for response spectra derived from Japanese strong-motion records accounting for tectonic source types. In *13th World Conference of Earthquake Engineering*, Vancouver, BC, Canada, paper 1271.
- Youngs, R. R., Chiou, S. J., Silva, W. J., & Humphrey, J. R. (1997). Strong ground motion relationship for subduction earthquakes. *Seismological Research Letters*, 68, 58–73.
- Zhao, J. X., Jiang, F., Shi, P., Xing, H., Huang, H., Hou, R., Zhang, Y., Yu, P., Lan, X., Rhoades, D. A., Somerville, P. G., Irikura, K., & Fukushima, Y. (2016a). Ground-motion prediction equations for subduction slab earthquakes in Japan using site class and simple geometric attenuation functions. *Bulletin of the Seismological Society of America*, 106, 1535–1551.
- Zhao, J. X., Liang, X., Jiang, F., Xing, H., Zhu, M., Hou, R., Zhang, Y., Lan, X., Rhoades, D. A., Irikura, K., Fukushima, Y., & Somerville, P. G. (2016b). Ground-motion prediction equations for subduction interface earthquakes in Japan using site class and simple geometric attenuation functions. *Bulletin of the Seismological Society of America*, 106, 1518–1534.
- Zhao, J. X., Zhou, S., Zhou, J., Zhou, C., Zhang, H., Zhang, Y., Gao, P., Lan, X., Rhoades, D. A., Fukushima, Y., Somerville, P. G., & Irikura, K. (2016c). Ground-motion prediction equations for shallow crustal and upper-mantle earthquakes in Japan using site class and simple geometric attenuation functions. *Bulletin of the Seismological Society of America*, 106, 1552–1569.
- Zhao, J. X., Zhang, J., Asano, A., Ohno, Y., Oouchi, T., Takahashi, T., Ogawa, H., Irikura, K., Thio, H. K., Somerville, P. G., Fukushima, Y., & Fukushima, Y. (2016d). Attenuation relations of strong ground motion in Japan using site classification based on predominant period. *Bulletin of the Seismological Society of America*, 96, 898–913.